Overview of the Fracture Network at Different Scales Within the Granite Reservoir of the EGS Soultz Site (Alsace, France)

Chrystel Dezayes, Albert Genter, Benoît Valley

Proceedings World Geothermal Congress 2010
Bali, Indonesia, 25-29 April 2010

Overview of the Fracture Network at Different Scales Within the Granite Reservoir of the EGS Soultz Site (Alsace, France)

Chrystel Dezayes[1], Albert Genter[2], Benoît Valley[3]

[1]BRGM, Geothermal Department, 3, avenue Cl. Guillemin, BP36009, F-45060 Orléans Cedex 2
[2]GEIE Exploitation Minière de la Chaleur, Route de Soultz, BP40038, F-67250 Kutzenhausen
[3]ETH Zürich, Engineering Geology, CH-8093 Zürich; now: MIRARCO/Laurentian University, 935 Ramsey Lake Road, Sudbury, ON P3E 2C6, CANADA
[1]c.dezayes@brgm.fr, [2]genter@soultz.net, [3]bvalley@mirarco.org

Keywords: Rhine graben, fractures, fracture zones, cores, borehole images, Enhanced Geothermal System

ABSTRACT

In EGS concepts like the one at Soultz, knowledge of the fracture network is essential to understand reservoir behavior and plan further stimulations and long term hydraulic circulation. At Soultz, the targeted reservoir is located at a 5km depth within the granite basement of the Upper Rhine Graben near the western border of France. This granite underwent a complex tectonic history including the Hercynian and Alpine orogeneses, leading to the currently observed fracturing. This fracturing is dominated by steeply dipping fracture sets which are distributed at various scales in the granite basement.

This structural work presents the characterization of the fracture network at different scales in order to understand and model the hydro-thermo-mechanical behavior of the granite geothermal reservoir through hydraulic stimulation and subsequent circulation tests. The small-scale fracture network has been characterized based on several kilometers of high resolution borehole image logs, allowing the characterization of different sets. There was a focus on large-scale fracture zones, which are the major fluid pathways. A total of 39 fracture zones have been described in detail based on borehole data. They have been compared to large-scale geophysical investigations using Vertical Seismic Profile (VSP) and passive microseismicity in order to build an extended fracture network in 3D. Hydraulically active fractures have been investigated in more detail in the different open-hole sections based on image logs, flow logs and temperature logs. These near-well borehole fractures represent potential fluid pathway for connecting the borehole to the far-field geothermal reservoir.

The fracture network in the granite Soultz reservoir is constituted by large-scale fracture zones, which are connected to a dense network of small-scale fractures. However, fluid pathways are more complex, with channelized structures, because only a limited number of fractures support fluid flow.

1. INTRODUCTION

Since 1980 (Gérard *et al.*, 1984; Gérard and Kappelmeyer, 1987), the goals of the EGS project at Soultz (France) have been to experiment and develop a new geothermal technology. After the initial Hot Dry Rock (HDR) concept of artificial fracture creation in a homogeneous rock by hydraulic fracturing was realized, the concept at Soultz has progressively evolved toward an Enhanced Geothermal System (EGS), where reservoir development involved the reactivation of pre-existing fractures in the granite (Evans *et al.*, 2005; Gérard *et al.*, 2006). Thus, a good knowledge and the geometrical characterization of the rock mass and particularly of the fracture network are essential for many reasons, from the optimization of the borehole design to the understanding of the flow distribution at depth. At Soultz, this fracture network is structured at different scales, from major fracture zones cross-cutting the granite batholith to intra-crystalline microfractures that induce weakness in the rock mass (Dezayes *et al.*, 2000).

Several studies have shown that some fracture zones are water-bearing prior to stimulation (Vuataz *et al.*, 1990; Genter *et al.*, 1995) and form the main flow channels after stimulation and during circulation (Evans *et al.*, 2005; Sanjuan *et al.*, 2006). These fracture zones are probably reactivated by shearing during hydraulic stimulation. Moreover, other fracture zones that were not permeable prior stimulation have been activated during stimulation and have been taken into account in this study.

Thus, fracture zones form the main potential fluid pathways connected to the dense network of meso-scale fractures to form the geothermal reservoir, which is about 1,125 km^3 in the upper reservoir and 8 km^3 in the deeper reservoir, based on induced micro-seismicity study (Cuenot *et al.*, 2006).

This paper presents a characterization of intermediate scale to the large-scale fracture zones in order to make a geometrical update of the fracture data base likely to support conductive fluid flow. Small-scale fracture distribution and characterization have been extensively studied (Dezayes et al., 2000; Genter at al., 2000). The goal of this study is to define the geometry of the fracture network for a better understanding of the fluid circulation in a deep fractured granite reservoir dedicated to geothermal exploitation. These results are used to model the hydraulic stimulations and circulations in the Soultz geothermal reservoir (Sausse *et al.*, 2009; Rachez et al., 2006; Rachez and Gentier 2008; Baujard and Bruel, 2005; Kohl and Megel, 2005) and to make geophysical interpretations or inversions (Place *et al.*, 2009; Schill and Geiermann, 2009).

2. GEOLOGICAL AND STRUCTURAL CONTEXT

The Soultz site is located within the Upper Rhine Graben, which is a Cenozoic rift structure belonging to the West European Rift System, as shown in the geological map of the Graben in Figure 1 (Ziegler, 1992). The filling sediments are marine and lacustrine limestones, marls and evaporites (including the petroleum layers of Pechelbronn) overlaying in unconformity the Jurassic limestones and the Germanic Trias (indicated by (b) in Figure 1-II). These Cenozoic and Mesozoic sediments have been deposited on the Paleozoic basement, which includes porphyritic monzo granite and two-mica granite (Genter *et al.*, 1999; Stussi *et al.*, 2002; Cocherie *et al.*, 2004; Hooijkaas *et al.*, 2006).

This granite unit is the target of the geothermal project and hosts the geothermal reservoir. This massif underwent a multiphase tectonic history, including the Hercynian and Alpine orogeneses. The Cenozoic tectonic history is reflected by the orientations of the current structures forming the Upper Rhine Graben (Figure 1). The regional major border faults mapped on the surface or derived from petroleum seismic reflection studies within the Upper Rhine Graben show a N0-30°E direction in relation to the three main directions of the graben (Figure 1). In the southern part of the graben, the main direction is about N10°E. This direction rotates clockwise at the center of the graben to N25°E-N30°E and becomes N0°E in its northern part. The Rhenish fracture orientation was formed during the Oligocene opening of the Rhine graben (Villemin and Bergerat, 1985), probably reactivating some Hercynian structures (Illies, 1972, Illies, 1975; Rotstein *et al.*, 2006). At the Soultz site, the Upper Rhine Graben rotates, and the regional border faults have a N45°E orientation. This direction is also present in the Triassic sediments in the Vosges area west of the graben fault (Ménillet et al., 1989).

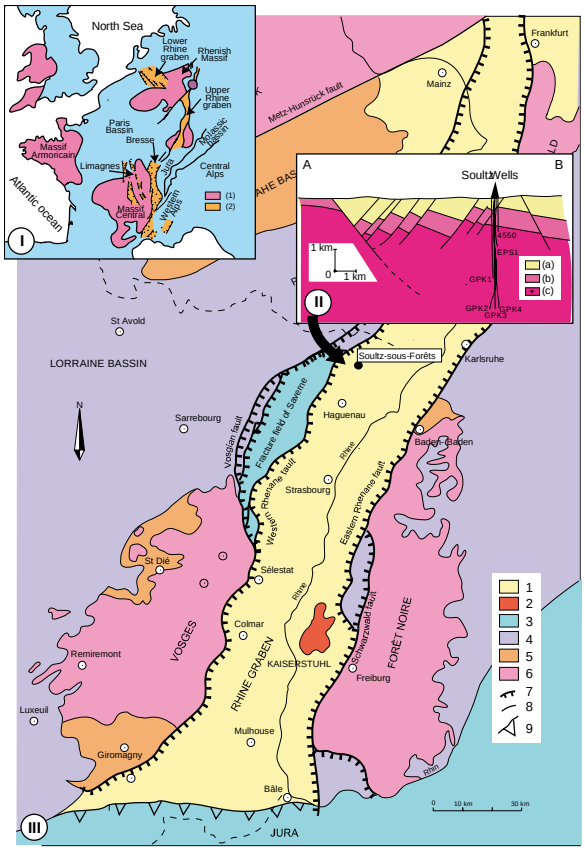

Figure 1: Location of the EGS Soultz site and geology of the Upper Rhine Graben. I) Location of the Upper Rhine Graben within the West European Rift System. (1) Hercynian basement; (2) Tertiary basins; (3) Alpine molasse. II): W–E cross-section through the Rhine Graben border and the Soultz site. (a) Cenozoic; (b) Mesozoic; (c) Hercynian basement. III) Geological and structural map of the Rhine graben. (1) Cenozoic sediments; (2) Cenozoic volcanics; (3) Jurassic; (4) Triassic; (5) Permo-Carbonifeous basins; (6) Hercynian basement; (7) boundary faults; (8) other faults; (9) overthrusts

However, the granitic basement has been affected by ante-Cenozoic tectonics, particularly the Hercynian orogen. The strike of the major dislocations delimiting the different Hercynian tectonic blocks is roughly N60°E (Figure 1). Geological mapping, borehole data and interpretation of seismic profiles acquired on a local scale around the Soultz site during the exploration of the Pechelbronn oil field provided lots of data to characterize the major fault system (Foehn, 1985; Place *et al.*, 2009). These data were compiled to build a 3D geological model of the sedimentary cover (Renard and Courrioux, 1994; Castera *et al.*, 2008). These studies show that in the sedimentary cover, the faults have a N20°E strike, i.e. a Rhenish direction (Figure 1). In map view, the faults have a trace length of about 2 to 20 km and occur with a spacing range of about 800 m to 3 km (Valley *et al.*, 2007). At depth, below the Soultz site, a horst structure is present, and the top of the basement is at a 1.4 km depth (Figure 1-II). Within this horst structure, some local faults were detected on the seismic profiles, which mainly dip to the west (Figure 1-II).

On the Soultz site, five boreholes have been drilled since 1987. Two relatively shallow, fully cored, exploratory wells called GPK1 and EPS1 were drilled to depths of 3600 m and 2200 m respectively. Three wells called GPK2, GPK3 and GPK4 were drilled for reservoir development and heat exploitation to depths of approximately 5000 m, where temperatures reach 200°C. (Baumgärtner *et al.*, 2004). These wells are illustrated in Figure 2. The exploitation triplet consists of GPK2, GPK3 and GPK4, which were drilled from the same well pad and are slightly inclined with depth. The three wells are aligned at 5000 m depth in a N165°E direction, and the horizontal distance between adjacent wells is about 700 m at depth (Figure 2).

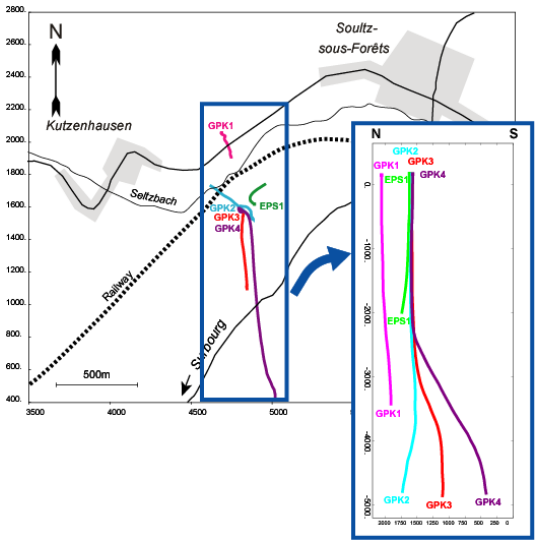

Figure 2: Map view and N-S cross-section of the EGS well trajectories at Soultz

3. METHODOLOGY

The orientation and classification of several thousand fractures were observed from oriented borehole images. High-resolution acoustic image logs such as BoreHole TeleViewer (BHTV) were acquired in GPK1 and EPS1, and Ultrasonic Borehole Imager (UBI) in GPK2, GPK3 and GPK4, as shown in Figure 3. Various electrical image logs (FMS, FMI, ARI) were run in the GPK1 and GPK2 wells and analysed in previous studies (Genter *et al.*, 1995; Dezayes *et al.*, 1995; Genter *et al.*, 1997).

In the cores, all the fractures are systematically sealed by hydrothermal filling but only 20% of them are visible on

the borehole images (Genter *et al.*, 1997). However, only the EPS1 borehole is fully cored (Figure 3) and some spot coring is available in GPK1 and GPK2. But the borehole images are suitable for detecting and measuring the orientation of the meso-scale fractures and fracture zones.

For the analysis of the small-scale fractures, two main types of fractures have been defined along the wells based on their origin: the natural fractures, which are older than the drilling and related to the tectonic history of the granite massif, and the induced fractures formed during the drilling that are related to the present-day stress field. In this study, only the natural fractures have been taken into account. Induced fractures have been studied in other papers like Tenzer *et al.* (1991), Genter *et al.* (1995), Dezayes *et al.* (1995), and Valley and Evans (2005).

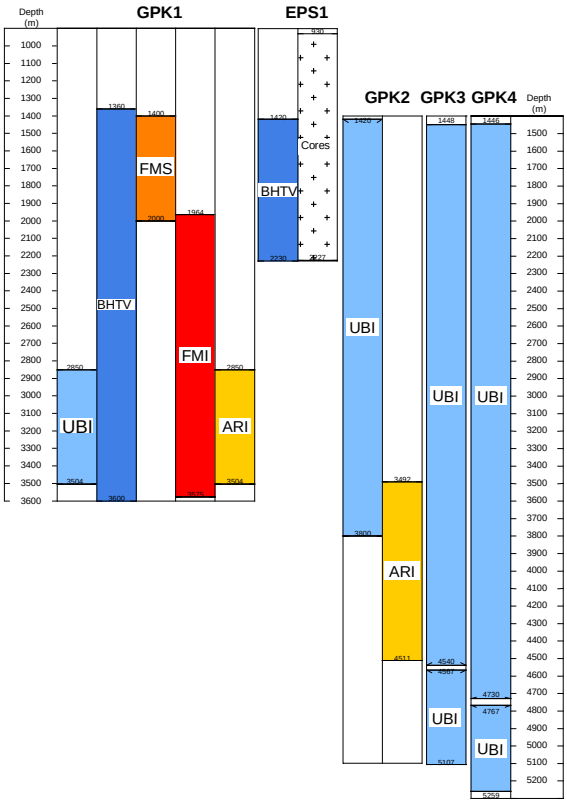

Figure 3: Core and image data available in the Soultz wells. BHTV: BoreHole TeleViewer; UBI: Ultrasonic Borehole Imager; FMS: Formation Micro Scanner; FMI: Fullbore Micro Imager; ARI: Azimuthal Resistivity Imager. Depth: measured depth along the well (MD)

The natural fracture typology was defined in order to obtain homogenous fracture datasets in the GPK3 and GPK4 wells (Dezayes *et al.*, 2005). This typology is based on two main criteria:

- The comparison of transit time and amplitude image logs can be used to determine if the fracture is open (dark traces) or not (no trace).
- The continuity of the sinusoidal trace on the amplitude image can be used to distinguish the scale of fractures (100% to 80% of the sinusoidal trace visible representing large fracture, between 80% and 50% and lower than 50% of the sinusoidal trace representing medium-sized fracture, and uncertain sinusoidal fitting representing small fracture). The occurrence of an alteration halo surrounding the fracture is also taken into account.

In order to better characterize low permeability fracture zones, the geological database was used based on petrographical descriptions of cuttings, borehole image log and geophysical log analyses, and caliper, spectral gamma ray and drilling parameters (Figure 4). The spectral gamma ray data, such as potassium, thorium and uranium contents, were used to detect radioactive element concentrations due to the hydrothermal alteration related to fracture zones or some petrographical variations.

However, evidence of natural permeability in a given fracture cannot be determined by interpreting geological data only. Thus, temperature and flow log analyses were used as well to determine the zone of fluid lost in the boreholes (Evans, 2000; Dezayes *et al.*, 2004).

On borehole images, fracture orientations are sometimes difficult to measure due to the fact that fractures are not perfectly planar as it is assumed for the dip calculation. Also, fracture zones are complex, and their orientation is difficult to define. Often, several individual fracture traces are visible on the log image within a given fracture zone, which includes brecciated to microbrecciated zones. To determine the overall orientation of a fracture zone, it was considered that the orientation of the border of the brecciated zone is representative of the overall orientation if this limit is clearly visible and defined and if it forms a well-marked planar structure. However, when several planar structures were present and roughly parallel, it was assumed that the orientation of the fracture zone is well approximated by the 3D average orientation of the individual parallel planes.

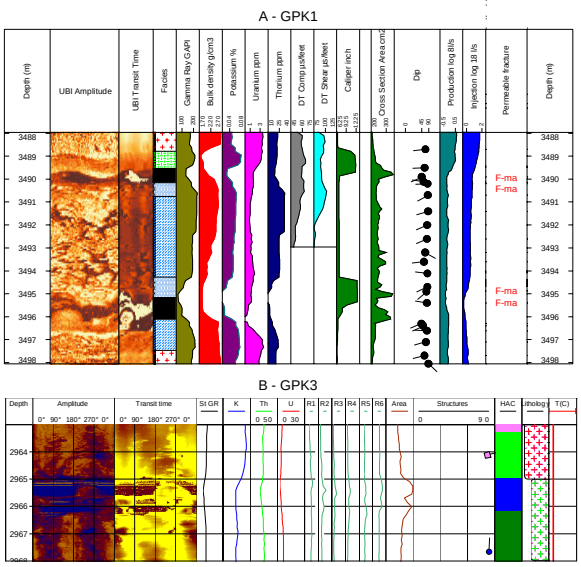

Figure 4: Example of synthetic combined logs for two fracture zones in GPK1 (A) and GPK3 (B)

In the open-hole sections of GPK3 and GPK4, several temperature and flow logs were acquired during the stimulation of the granite reservoir. The detailed studies of these logs coupled with the borehole image logs enabled the definition of the fluid exit zone, which connected the wells with the reservoir.

4. MESO-SCALE FRACTURES

Fracture Orientation

Many fracture data have been collected in the granite basement based on coring and especially borehole imaging (Genter *et al.*, 2007). The analyses of these fracture data show that the main strike is consistent between the different imagery logs and the different wells, as is illustrated in Figure 5 (Genter, 1989; Genter *et al.*, 2000; Dezayes *et al.*, 2004).

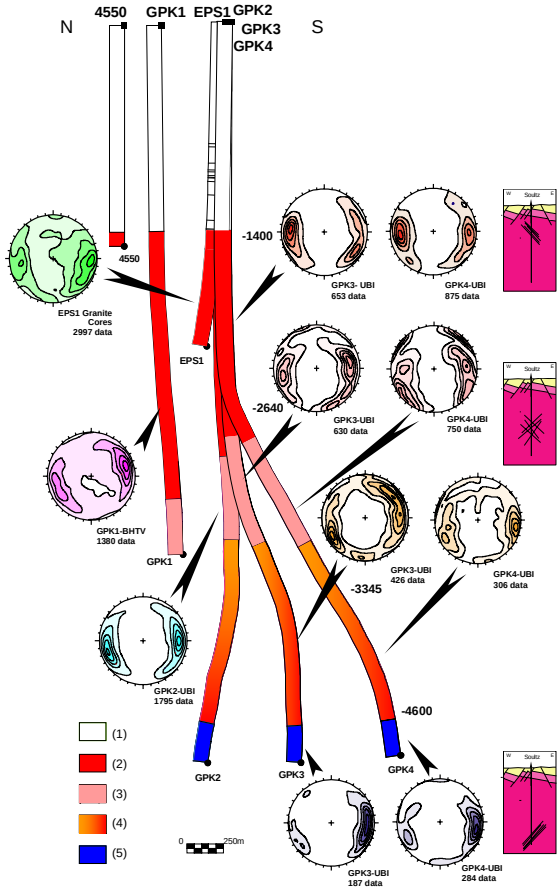

Figure 5: Fracture orientation in relation to the major petrographical crystalline sections in GPK3 and GPK4: (1) Sedimentary cover, (2) standard porphyritic granite, (3) Standard granite with intense vein alteration, (4) Biotite and amphibole rich granite gradually becoming standard granite with depth, (5) Two mica granite and biotite rich granite. The depths along the wells indicate the upper and the lower depth limits of the petrographical sections (in True Vertical Depth, from the drilling floor). Contour-density diagrams of all fracture types in Schmidt's projection, lower hemisphere: 10%, 30%, 50%, 70%, and 90% of the maximum frequency

In EPS1, the coring began at 920 m in the lower Muschelkalk. In the granite, the major direction varies from N160°E to N-S with steep dipping eastward and westward. However, the orientations of fractures observed in cores (EPS1) are rather scattered with various dipping values (Figure 5). In these cores, some faults showing striations have been measured and the Oligocene paleostress states have been retrieved by inversion (Dezayes *et al.*, 1995). Among the fractures in granite, seven sets have been isolated using a statistical method based on borehole image interpretation (Valley, 2007). 60% of fractures belong to two sets striking N-S and dipping to the west and to the east. This orientation corresponds to the Rhenish orientation described on graben and site scales. A sub-vertical set, striking NW-SE, also appears on a large scale outside of the Rhine graben in the Vosges and Black Forest massif and in the Triassic sediments. Another subvertical perpendicular set, striking NE-SW, is parallel to the Hercynian large scale faults, like the Lalaye-Lubine-Baden-Baden fault. These four sets include 95% of all fractures found in granite (Valley, 2007). It appears clearly that the granite batholith has recorded a polyphased tectonic history. With depth, the strike of the main N-S sets remains roughly similar; however, balance evolved between the dominant dip orientation (Figure 5). In GPK3 and GPK4, between 1420 m to 2700 m TVD (True Vertical Depth), the main fracture set dips to the east. In the middle part of the borehole sections, between 2700 m to about 4800 m TVD, the two conjugate sets are equally represented with fracture sets dipping westward and eastward. In the bottom part of the wells, below 4800 m to 5000 m TVD, the westward set is dominant (Figure 5).

Density

In the GPK3 and GPK4 wells, where we have a continuous fracture data set, the cumulative density of fractures has been computed along the well trajectories respectively. This density is a linear density along a subvertical sampling, where fractures are subvertical. The absolute values of density are then underestimated in relation to the real 3D density of fractures and are minimum values. On the other hand, the relative values and the density variations are both significant. Nine sections with variable density values alternate with depth, as shown in Figure 6.

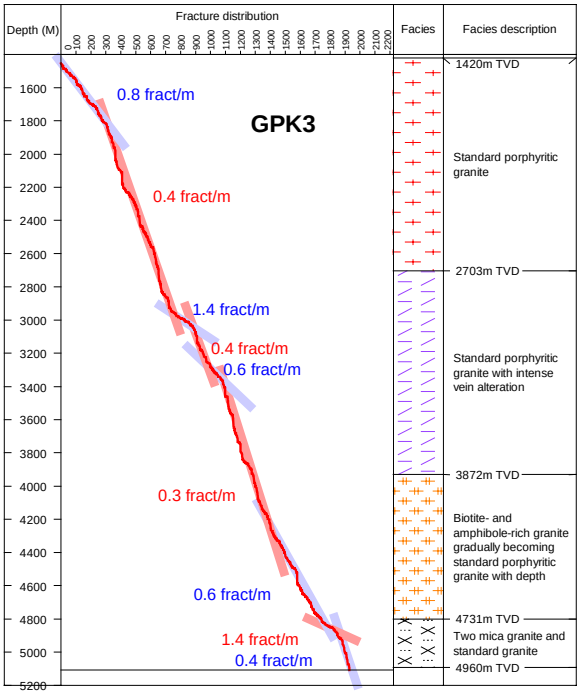

Figure 6: Cumulative number of fracture with depth including all fracture types derived from borehole image analysis in the GPK3 well. Depth in the left column corresponds to the measured depth along the borehole from the drilling floor. The depth boundary of the granite facies in the right column corresponds to the vertical depth from the drilling floor

In the GPK3 well, the high density value (0.8 fract./m) observed in the upper part of the granite is in agreement with the previous studies done at Soultz (Genter *et al.*, 1997). From 1800 m to about 2900 m, the fracture density is quite constant, with a low density (0.4 fract./m). These two sections correspond in terms of petrography to the standard pophyritic granite (Hooijkaas *et al.*, 2006; Figure 6).

In the intermediate part of the well, two high fracture density zones (1.4 fract./m and 0.6 fract/m) surround a low density zone (0.4 fract./m). These three zones correspond to the upper part (between 2900 m and 3300 m MD) of the highly fractured and altered standard granite facies (Figure 6).

Below these zones, there are two low and moderate fracture density zones, which are embedded into the biotite and amphibole rich granite (Figure 6).

In the lower part of the well (from 4800 m MD), a very high fracture density zone occurs. This zone corresponds to the boundary between two granite facies: the standard porphyritic granite and the two-mica granite. In this deep fine-grained facies, the fracture density is very low and decreases significantly to 0.4 fract./m (Figure 6).

In the neighboring GPK4 well, a high density value (0.8 fract./m) occurs in the upper part of the granite, as in the GPK3 well. Between about 1800 m and 1900 m MD, the fracture density increases to 1.25 fract./m. Below 1900 m and to about 2700 m, the fracture density is quite constant with a low density (0.55 fract./m). These three sections correspond in terms of petrography to the standard porphyritic granite and are illustrated in Figure 7.

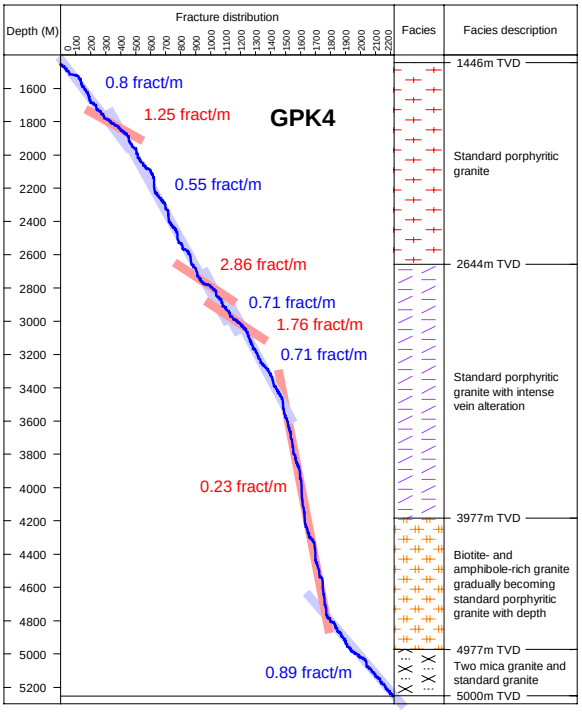

Figure 7: Cumulative number of fractures with depth including all fracture types derived from borehole image analysis in the GPK4 well. Depth in the left column corresponds to the measured depth along the borehole from the drilling floor. The depth boundary of the granite facies in the right column corresponds to the vertical depth, from the drilling floor

In the intermediate part of the well, two very high fracture density zones (2.86 fract./m and 1.76 fract/m) alternate with two moderate density zones (0.71 fract./m). These four zones correspond to a highly fractured and altered standard porphyritic granite facies, between 2900 m and 3500 m MD (Figure 7).

Below these zones, between 3500 m and 4750 m MD, the fracture density is very low and quite constant with a value of 0.23 fract/m (Figure 7).

In the lower part of the well (from 4750 m MD to the bottom of the well), a high fracture density zone (0.89 fract./m) occurs in the lower part of the biotite and amphibole rich granite facies and the two mica-granite (Figure 7).

5. FRACTURE ZONE NETWORK

Characterization of Fracture Zones

In the six wells of the Soultz site, 39 fracture zones were considered, which indicate some potential traces of fluid flow, as shown in Table 1 and Figure 8. This list of fracture zones is probably not exhaustive and could be completed later by further data acquisition or processing.

Table 1. All fracture zones determined in this study. TVDss: True Vertical Depth Sub Sea. Depth: measured depth along the well. Fracture zones of level 1 are bold; fracture zones in level 2 are normal text; fracture zones in level 3 are italicized.

Well	Name	Depth	Level	TVDss
EPS1	*EPS1-FZ1010*	*1012*	*3*	*836.637512*
EPS1	**EPS1-FZ1200**	**1198**	**1**	**1021.84821**
EPS1	EPS1-FZ1640	1643	2	1466.48914
EPS1	**EPS1-FZ2180**	**2179**	**1**	**1988.09058**
GPK1	*GPK1-FZ1015*	*1015*	*3*	*862.00885*
GPK1	**GPK1-FZ1220**	**1220**	**1**	**1066.59717**
GPK1	**GPK1-FZ1820**	**1820**	**1**	**1666.24219**
GPK1	GPK1-FZ2815	2815	2	2657.19238
GPK1	*GPK1-FZ3220*	*3223*	*3*	*3064.05273*
GPK1	GPK1-FZ3490	3492	2	*3332.64502*
GPK2	**GPK2-FZ2120**	**2123**	**1**	**1953.37292**
GPK2	*GPK2-FZ3240*	*3242*	*3*	*3069.90625*
GPK2	*GPK2-FZ3350*	*3347*	*3*	*3174.62988*
GPK2	*GPK2-FZ3515*	*3514*	*3*	*3341.70801*
GPK2	GPK2-FZ3900	3900	2	3726.61133
GPK2	GPK2-FZ4760	4760	2	4544.82227
GPK2	*GPK2-FZ4890*	*4890*	*3*	*4668.3252*
GPK2	GPK2-FZ5060	5060	2	4831.29248
GPK3	*GPK3-FZ1580*	*1579*	*3*	*1410.36487*
GPK3	*GPK3-FZ1640*	*1637*	*3*	*1468.78821*
GPK3	*GPK3-FZ1820*	*1820*	*3*	*1651.01147*
GPK3	*GPK3-FZ2040*	*2042*	*3*	*1873.30823*
GPK3	*GPK3-FZ2045*	*2046*	*3*	*1876.76367*
GPK3	*GPK3-FZ2090*	*2092*	*3*	*1923.16223*
GPK3	*GPK3-FZ2970*	*2970*	*2*	*2798.43579*
GPK3	GPK3-FZ3270	3271	2	3092.95361
GPK3	*GPK3-FZ4090*	*4089*	*3*	*3856.2417*
GPK3	**GPK3-FZ4770**	**4775**	**1**	**4538.90137**
GPK4	*GPK4-FZ1720*	*1723*	*3*	*1554.30212*
GPK4	*GPK4-FZ1800*	*1801*	*3*	*1632.22925*
GPK4	*GPK4-FZ2820*	*2817*	*3*	*2762.20264*
GPK4	*GPK4-FZ3940*	*3940*	*3*	*3603.97852*
GPK4	*GPK4-FZ4360*	*4361*	*2*	*3963.29565*
GPK4	*GPK4-FZ4620*	*4620*	*3*	*4195.97852*
GPK4	GPK4-FZ4710	4712	2	4279.59717
GPK4	*GPK4-FZ4970*	*4973*	*3*	*4530.36914*
GPK4	*GPK4-FZ5050*	*5012*	*3*	*4568.51904*
GPK4	*GPK4-FZ5100*	*5100*	*3*	*4655.44922*
4550	**4550-FZ1265**	**1265**	**1**	**1107.95679**

The fracture zones have been classified within three levels in attempting to reflect their relative scale and importance

as fluid flow paths. The first level (1 in the Table 1) concerns the major fracture zones, which have been detected during drilling operations with important mud losses and were permeable prior to any stimulation operations. The fracture zones of the second level (2 in the Table 1) show flow indication higher than 20% of water losses during stimulation and/or are characterized by the other available geological data to include at least one thick fracture accompanied with a significant halo of hydrothermal alteration. The last level (3 in the Table 1) includes the fracture zones having a poorly developed alteration halo and a flow level below 20% of water losses during stimulation. This level indicates fracture zones of smaller size than those of the two other levels previously defined.

In the three wells EPS1, GPK1 and 4550 (a monitoring seismic well), a major fault zone intersected those wells within the Buntsandstein sediment at around 1200 m (Table 1). This zone has been cored by the EPS1 well and where it forms a large structure containing 3 sub-zones and fractures with quartz, galena and barite fillings. In the GPK1 and 4550 wells, total drilling mud losses occurred when drilling through this zone (Herbrich, 1988; Villeneuve and Weber, 1991). In the 4550 well, a BHTV log is available and allows characterization of the fracture zone. This presents a series of open steeply dipping fractures. However, the orientation value is not very precise due to the rather bad quality of the image log.

In the GPK1 well, another natural brine inflow occurred during the drilling at a depth of 1820 m MD in the large fracture zone listed in Table 1 (Herbrich, 1988). At this depth, a very high helium content anomaly was recorded (Vuataz *et al.*, 1990), and other drilling anomalies were reported. This fracture zone contains geodic quartz veins that are visible in a core taken at this depth as well as illite (Genter, 1989).

Also, a fracture zone provoking total drilling mud losses was intersected in the upper part of the granite in well GPK2, and no cuttings were collected below (Genter *et al.*, 1995). The fracture zone at 2120 m MD is a highly altered zone with several open fractures (Table 1). The hydraulic testing of an open hole interval including this fracture zone showed that 95% of the flow rate was absorbed by this zone (Jung *et al.*, 1995). This zone is also believed to be responsible for a large-scale stress perturbation, as highlighted by the analysis of borehole failure (Valley, 2007).

There are no major fracture zones at greater depths except at the bottom of the GPK3 well, in which there is a major fracture zone within the open hole located around 4770 m MD (Table 1). This zone includes several individual fractures with a cumulative apparent thickness of around 15 m along the well. The K content increases in the hanging wall of the zone and decreases in the central part, indicating a high alteration halo. Flow rates indicate a 70% outflow matching this zone (Dezayes *et al.*, 2004). Analysis of borehole failure showed that this zone is inducing a major stress perturbation (Valley, 2007). This is the major flow pathway in the geothermal reservoir at lower depths. GPK4 is the only well where there is no level 1 fracture zone (Table 1). The description of the fracture zones is detailed by Dezayes and Genter (2008).

The orientation of these fracture zones is based on borehole images, as is described above (Figure 8). Most of orientations of fracture zones were determined according to the assumptions cited above. However, some of them are more difficult to estimate and are detailed in the following text. The orientation of the fracture zone in GPK3 at 3270 m, which appears to strike E-W (Figure 8D, Table 1), is very imprecise. The image log quality is locally poor, and no corrective measures have been enacted. Moreover, the orientation of some fracture zones in GPK2 could not be measured at all. This well was drilled twice (in 1995 and 1999) and some problems occurred at 3900 m, where the first drilling stopped. Based on the caliper log, it seems as if a large cave occurs at that depth (Genter *et al.*, 1999). Some altered cuttings coming from this zone were recovered at the end of the drilling operation in 1995. As this large cave occurs in a significantly deviated part of the well, the UBI tool stuck after the deepening in 1999, and no image log could be run below that depth. The borehole was cased later, and the presence of a casing restriction is now suspected due a partial casing collapse induced by the fracture zone. Based on 3D visualization (Sausse *et al.*, 2009), this fracture zone is considered to be the same one that cross-cuts the bottom of well GPK3 (GPK3-FZ4770 in Table 1). Thus, it was assumed that this zone has the same orientation (Table 1). However, due to this GPK2 borehole wall restriction at 3900 m, no logging tools could be run below this depth. Only temperature and flow logs are available below 3900 m. Then, three zones with outflow were located which match the altered zones based on cutting observations. These zones occur at 4760 m with 20% of flow, 4890 m with 17% of flow and below 4960 m with 50% of flow, which could correspond to a fracture zone occurring at 5060 m MD, based on cutting observations. As there are no oriented image logs in this section, a generic orientation of N250°E-65° (N160°E-65°W) was assumed for the dominant orientation of fractures in the deeper part of the Soultz granite, which is realistic but not proven (Figure 8C).

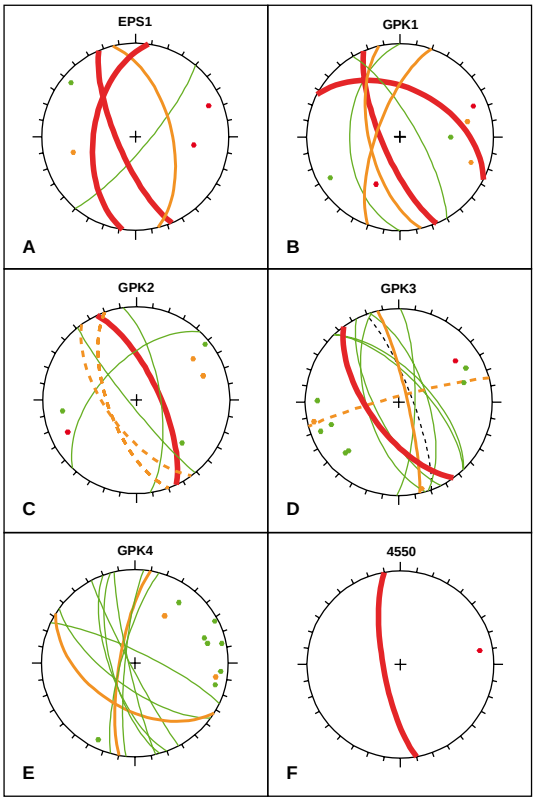

Figure 8: Orientation of fracture zones in each Soultz well. Red lines and red dots: cyclographic traces and poles of fracture zones of level 1; orange

lines and orange dots: cyclographic traces and poles of fracture zones of level 2 (dotted orange line: supposed orientation); green line and green dot: cyclographic traces and poles of fracture zones of level 3 (Schmidt's projection, lower hemisphere)

Organization of the Fracture Zones

Most of the fracture zones characterized in the framework of this study (Table 1) can be attributed to three main clusters of fracture zones at about 1800-2000 m, 3000-3400 m and 4500-5000 m TVD (True Vertical Depth), as illustrated in Figure 9. In that regard, the GPK4 borehole is somehow atypical, presenting less clearly clustered, steeply dipping fractures (Figure 9). In the other wells, fracture zones more consistently correspond to these three fracture zone clusters. This was reported previously in the upper part of the granite body, before the deepening of GPK2 and the drilling of GPK3 and GPK4 (Genter *et al.*, 1995; Genter and Castaing, 1997). These three clusters of fracture zones are considered to reflect a major fault, equivalent to the fault detected in the sedimentary cover based on seismic reflection (Genter and Castaing, 1997). If it is assumed that these faults are steeply dipping structures with values higher than 60°, the raw spacing between two consecutive clusters of fracture zones is around 500 m, which is equivalent to the fault spacing in the sedimentary cover (Valley *et al.*, 2007).

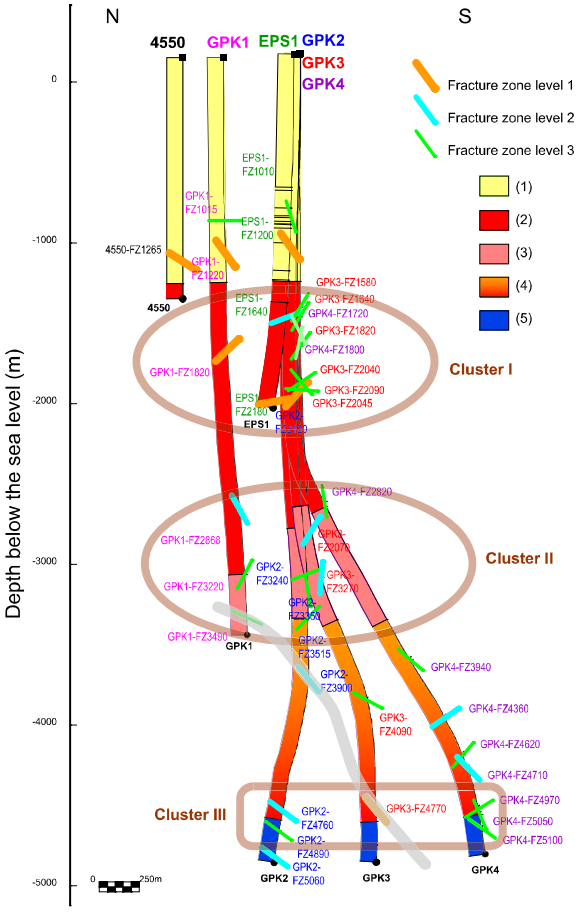

Figure 9: Synthesis of the all fracture zones determined in this study along a N-S cross-section through the Soultz wells. (1) Sedimentary cover, (2) standard porphyritic granite, (3) Standard granite with intense vein alteration, (4) Biotite and amphibole rich granite gradually giving way to standard granite with depth, (5) Two mica granite and biotite rich granite

The upper cluster at 1800-2000 m depth MD (Cluster I in Figure 9) is located in the unaltered porphyritic granite. This cluster includes major fracture zones qualified as level 1 with permeable zones. The cluster II does not include major level 1 faults. It is located within the fractured and altered granite zone (Figure 9). This granite facies is characterized by high pervasive alteration related to numerous meso-scale fractures present in this zone (Hooijkaas *et al.*, 2006). This facies contains a high proportion of clay and hydrothermal minerals. The high fracturing of this facies possibly leads to a generally weaker rock mass, where the strain is distributed in small increments over a dense network of smaller fractures, instead of being concentrated by a few major faults. This location corresponds to the upper reservoir stimulated in the first phase of the project in 1997 (Baumgärtner *et al.*, 1996). In this reservoir, a four month circulation loop test with tracer injection was performed with success (Bruel, 2002). Based on this test, it appears that there is a good fluid connection in this reservoir between GPK1 and GPK2. The lower cluster (Cluster III in the Figure 9) is close to the interface between the 2 granite units at 4700 m TVD. The deep facies is characterized by massive granite with a low degree of pervasive alteration. Cluster III contains major fracture zone (GPK3-FZ4770 in Table 1). Thus, it appears that the deformation in this facies tends to be localized along major isolated fracture zones. This last cluster is located in the lower reservoir, which was stimulated previously and is currently a part of the deep geothermal loop under testing for the electrical production test. Conceptually, this reservoir appears to behave as a fractured reservoir embedded in a low permeability matrix.

Based on this characterization of fracture zones at a borehole scale, these major planes have been compared to other fracture information derived from other detection methods in order to build a 3D model (Sausse *et al.*, 2009). These other methods are microseismicity data collected within the reservoir during the stimulations of GPK2, GPK3 and GPK4 (Dorbath *et al.*, 2009) and a VSP (Vertical Seismic Profiling) investigation (Place *et al.*, 2009). Some of the fracture zones observed at the well scale match the microseismicity or VSP results. They correspond to fracture zones qualified by level 1 or 2 such as GPK1-FZ3490, GPK2-FZ3900 and GPK3-FZ4770, which match microseismicity and VSP analysis. Moreover, the dip orientations of the fracture zones are very close and seem to define a large-scale fault intersecting the Soultz basement (Figure 9). The orientation of these major fracture zones is about N230°E-70° (N140°E-70°W).

In GPK1, two fracture zones at 1820m MD and 2860m MD appear to match with the VSP analysis (Place *et al.*, 2009; Sausse *et al.*, 2009).

In the lower part of the reservoir, two smaller fracture zones in GPK4 match geometrically with the microseismicity analysis at 4620 m and 4970 m MD (Sausse *et al.*, 2009). These fracture zones strike N10°E and dip steeply to the west (Figure 9).

6. FLOW PATTERN IN THE OPEN HOLE SECTIONS

Some of the fluid exit zones in the open holes correspond to fracture zones, such as the large ones in GPK3 at 4770 m MD describe above. In this well, six other zones have been defined as fluid exit zones. These exit zones are described

in Figure 10. They correspond to significant variations visible on the geophysical logs, but with lower amplitudes. However, the occurrence of hydrothermal alteration associated with these fractures is not well constrained. Chemical fluid variations observed in the drilling mud do not always match the permeable zones (Figure 10). Moreover, the zone at 4670 m MD revealed the presence of tracers, but did not seem to correspond to a fluid pathway during hydraulic testing (Sanjuan *et al.*, 2005).

Analysis of UBI data allows the determination of the orientation of open fractures located at the depth of the permeable zones observed from temperature and flow logs. The orientation and nature of the fracture zones vary in an important way. The most important zone at 4775 m MD, which takes 63% to 78% of fluid during the stimulation, is actually a cluster of fractures. The fractures within this cluster trend N160°E and most of them dip westward at an average angle of 52° (Figure 10).

The zone at 4875 m MD consists of four fractures, one of which appears thicker on the borehole images. The average orientation is N150°E-75°E. This zone takes 2% of the fluid during the stimulation tests. Chemical fluid variations and tracers observed from changes in the drilling mud indicate the presence of fractures bearing flow.

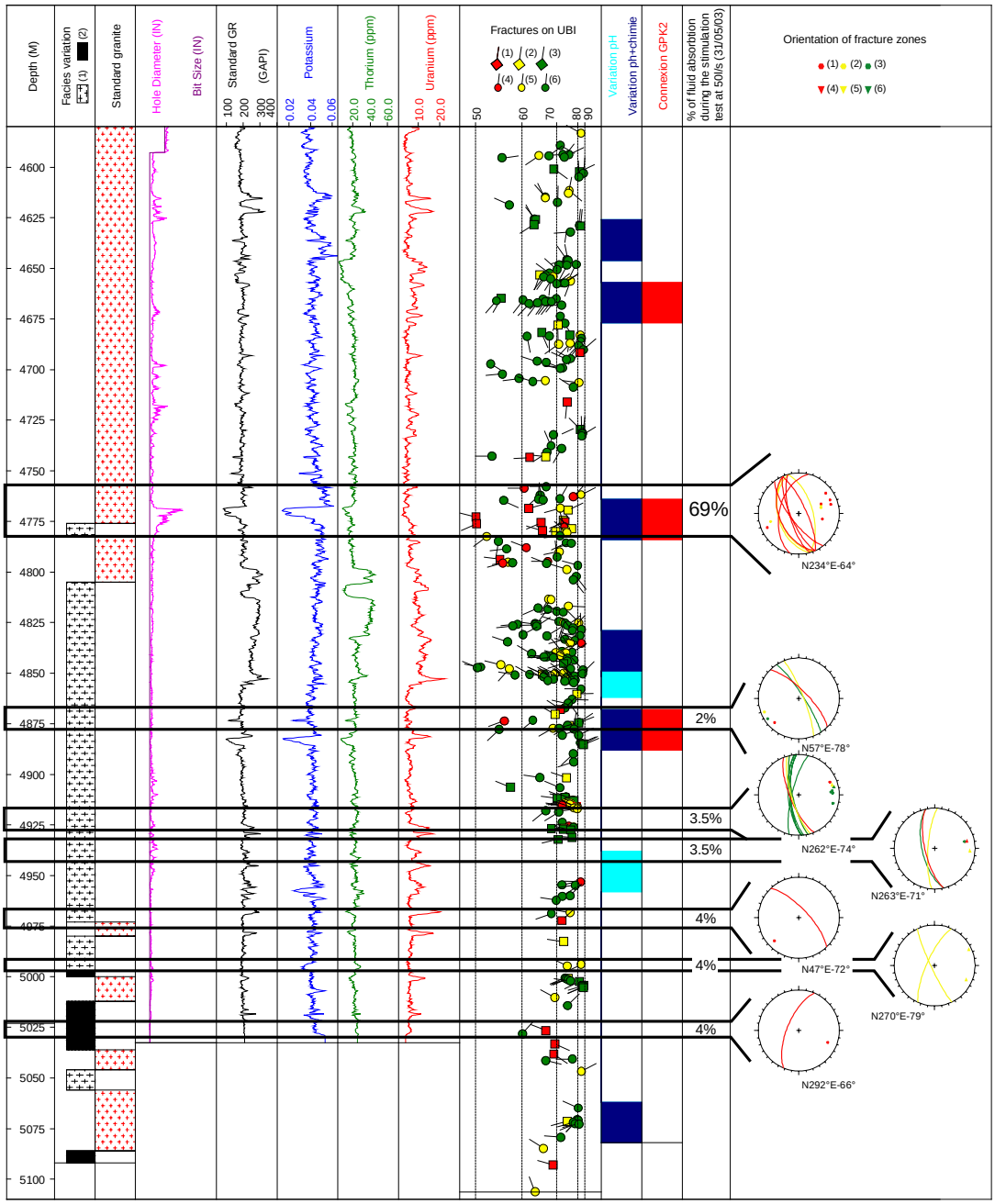

Figure 10: Synthetic log of the open hole section of the GPK3 well showing characterization of the fluid exit fractures. Column 2: Facies variation log: (1) two mica granite, (2) biotite rich granite; Column 3: Standard granite: porphyritic MFK-rich granite; Column 9: Open fractures versus depth: grey density variation indicates the percentage of continuity of the fracture trace on UBI log: (1) 100%, (2) >50%, (3) <50%. The horizontal scale indicates the dip value of fractures. The direction of the tadpole indicates the dip direction of fractures (north is to the top, east is to the right). Columns 10 and 11: Chemical fluid anomalies detected in the drilling mud flowing into and out of the drill hole

The zone at 4920 m MD also consists of several fractures, one of which stands out (Figure 10). This zone did not take any fluid during the last hydraulic test, which included injection at a rate of 50 l/s after two peaks at 90 l/s. The average orientation is N12°E-68°W (Figure 10). The zone at 4972 m MD showed a single open fracture without any alteration. The fracture is oriented N135°E-65°E and took approximately 4% of the fluid during all of the hydraulic tests. A deeper zone at 5025 m MD also consists to a single fracture oriented N22°E-58°W (Figure 10). The fracture takes 10 to 15% of the total injection accepted by the wellbore during all the hydraulic tests.

Two zones, namely 4940 and 4990m MD, do not correspond to open fractures based on UBI image logs acquired shortly after the end of the drilling. However, these two zones appear to be hydraulically active under certain conditions. The zone at 4940 m MD accepted about 2-4% of the injected fluid at injection rates of 25 and 30 l/s, but it did not accept any fluid during injection at 50 l/s or after the 90 l/s period. The zone at 4990 m MD seemed to be closed at the beginning of the stimulation (at an injection rate of 25 l/s), but later accepted 4% of the fluid flow. These zones may have initially been closed but were later re-opened during the hydraulic experiments.

In GPK4, as the flow logs have a bad quality, we based the determination of the fluid exit zones on the temperature analysis. The temperature variation was located, and fractures were characterized matching depth on borehole images. Then, nine fluid exit zones were determined, as shown in Figure 11. As there were less data than in GPK3, the zones in GPK4 are less constrained, and three degrees of fluid exit zones were used to describe them: certain, probable, and supposed (Figure 11). Three of them (ZA3, ZA5, and ZA7) were in the global fracture zone network.

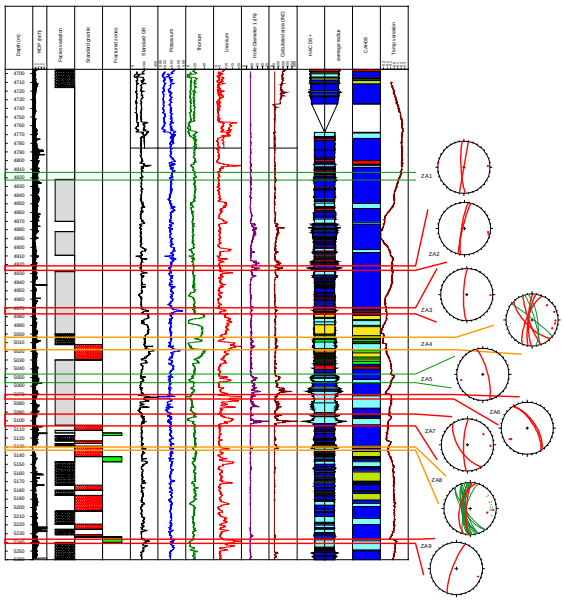

Figure 11: Synthetic log of the open hole section of the GPK4 well showing characterization of the fluid exit fractures. Column 2: Rate of Penetration. Column 3: Facies variation log: (1) two mica granite, (2) biotite rich granite; Column 4: Standard granite: porphyritic MFK-rich granite; Column 5: Occurrence of minerals indicating fracture zones; Column 6: Standard Gamma ray; Column 7: Potassium content; Column 8: Thorium content; Column 9: Uranium content; Column 10: hole diameter; Column 11: hole area; Column 12-14: HAC; Column 15: temperature variation

Five zones were described as “certain” fluid exit zones at 4923 m, 4973 m, 5073 m, 5100 m and 5238 m MD. At 4923 m MD, two N-S high dipping fractures are associated with the borehole cave and that kind of breakout (Figure 11). A 4973 m MD, one N-S high dipping fracture is present with a 1 m thick alteration halo on the both sides of the fracture. This alteration is also indicated by a high potassium and uranium content (Figure 11). A series of NW-SE parallel fractures forms the zone at 5073 m MD that exhibited a Gamma Ray anomaly. The potassium and thorium contents were found to be very low here, whereas the uranium content was high (Figure 11). At 5100 m MD, a brecciated zone is present with N-S and NNW-SSE borders. This zone is associated to a cave, observed on the caliper log, with low thorium content and high uranium content (Figure 11). The deeper zone at 5238 m MD is a series of several NNE-SSW parallel fractures. This zone has been detected with the cutting observations and presents a high uranium content (Figure 11).

The “probable” fluid exit zones are located at 5010 m and 5135 m MD. The first one is a large 15 m thick zone with many fractures. The average direction of these fractures is NNW-SSE with a high dip. This zone is characterized by high uranium content (Figure 11). At 5135 m MD, there is a series of fractures with a NNW-SSE average direction (Figure 11).

The two other zones were “supposed” exit zones. At 4822 m MD, two N-S high dipping fractures were present, but did not exhibit Gamma Ray anomaly (Figure 11). A cave was detected at 5050 m MD associated with high uranium content (Figure 11). N-S oriented fracture exits occurred that were associated with a kind of large breakout.

DISCUSSION

The average strike direction of fracture zones characterized in the granite is N160°E±15°, as shown in Figure 12. Two secondary sets are present with N20°E±10° and N130°E±10° directions. The average dip is higher than 60° in a dominantly westward direction (Figure 12). The orientation of meso-scale fractures measured in the granite on the borehole images and the cores was N175°E±30° with more fractures dipping to the west (Figure 12).

If the orientation of the fracture zones is compared to the meso-scale fractures, a clockwise rotation of 10-15° can be observed (Figure 12). However, the west dipping direction dominates in all cases.

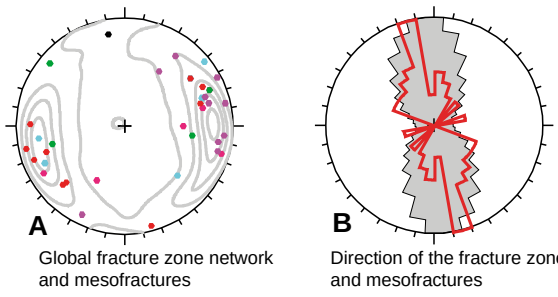

Figure 12: Synthesis of the orientation of fractures at different scales in the Soultz granite. A- Poles of fracture zones from the different wells (Green: EPS1, pink: GPK1, blue: GPK2, red: GPK3,

purple: GPK4, black: 4550) superimposed on a frequency contouring diagram of the mesofractures observed in the all Soultz wells (in grey 7433 data). B- Rose diagram of the fracture zones in red (34 data) and mesofractures observed in the all Soultz wells in grey (7433 data). (Schmidt's projection, lower hemisphere, rose diagram: 10° class angle, contouring diagram: 10%, 30%, 50%, 70%, 90% of the maximum frequency)

The fluid exit zones determined in the open hole sections of GPK3 and GPK4 showed nearly vertical fracture zones with a dominating N-S set dipping westward as well as a secondary NW-SE set dipping eastward (Figure 13). These orientations fit with a slightly clockwise rotation with the global orientation of the meso-fractures measured in the open hole sections (Figure 13). In this part of the granite, the main fracture set dips to the west.

In previous studies, these fracture zone concentrations were interpreted as the occurrence of large-scale normal fault zones related to the Rhine graben tectonics. However, the directions of the fracture zone and the meso-scale fractures are slightly different from the major fault orientation observed in the sedimentary cover, which has a Rhenish direction of N20°E and corresponds to the graben opening at Oligocene. The granite contains numerous fracture orientations related to Hercynian and Alpine tectonics. It seems that the N160°E is an inherited direction, which was reactivated during the graben tectonic activity. Thus, the main fracture zone orientation is rather different from those newly created in the sedimentary cover during the Cenozoic.

Moreover, the average direction of the fracture zones is rather consistent with the present-day stress field with σ_H N169°E±14°, one circular standard deviation (Klee and Rummel, 1993; Valley and Evans, 2007). Some fracture zones which show flow anomalies or indications of shearing appear as small fractures on the borehole image logs. This seems to indicate that critically oriented fractures relative to the stress state orientation could shear during hydraulic stimulation (Evans, 2005).

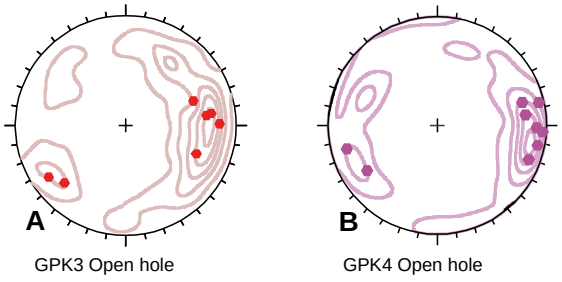

Figure 13: A- Poles of the fluid exit zones superimposed on the frequency diagram of mesofractures (349 data) in the open hole of GPK3. B- Poles of the fluid exit zones superimposed on the frequency diagram of mesofractures (349 data) in the open hole of GPK4. (Schmidt's projection, lower hemisphere, rose diagram: 10° class angle, contouring diagram: 10%, 30%, 50%, 70%, 90% of the maximum frequency)

CONCLUSIONS

The characterization of fractures at different scales was achieved along the Soultz wells based on direct (cores, cuttings) and indirect (borehole images, geophysical logs, flow logs, temperature logs) methods. Among the thousand fractures detected and measured, a set of 39 fracture zones were highlighted intersecting the five boreholes of the geothermal site as well as a peripheral well. This list is not extensive and could be completed using further data acquisition or processing. In the open hole sections of GPK3 and GPK4, 7 fluid exit zones were determined, and 9 were characterized. In GPK2, some exit zones have been detected, but no image logs are available to perform a geometrical characterization.

In a previous study, these fracture zone concentrations were interpreted as the occurrence of large-scale normal fault zones related to the Rhine graben tectonics, as shown in Figure 14. However, the direction of the fracture zone is slightly different from the major fault orientation observed in the sedimentary cover, which has a Rhenish direction of N20°E corresponding to the Oligocene graben formation. The granite contains fractures with numerous directions related to Hercynian and Alpine tectonics. It seems that the N160°E direction was an inherited and was reactivated during the graben tectonics. Thus, the main fracture zone orientation is rather different from those purely created in the sedimentary cover during the Tertiary. A 3D large-scale geometrical model is being built to highlight the relationship between the major faults in the sedimentary cover and the fracture zone clusters. This is an on-going work based on an exhaustive geological database (Castera *et al.*, 2008; Sausse *et al.*, 2008).

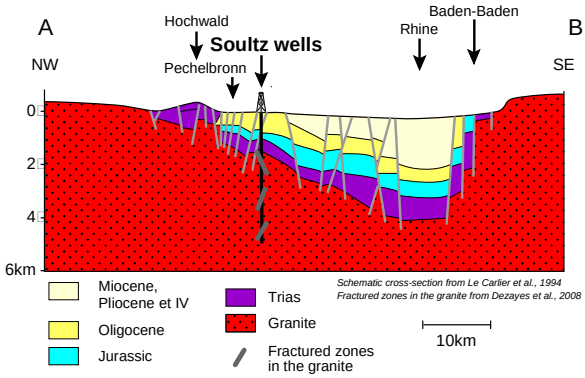

Figure 14: Schematic NW-SE cross-section (from Le Carlier et al., 1994) and location of the three fracture zone clusters in the Soultz well, represented with an average orientation

Knowledge and in situ characterization of fracture zones along the well have to be taken into account for a better understanding of the lifetime of the geothermal reservoir during early stages of hydraulic or chemical stimulations and subsequent long-term hydraulic circulations. Due to such hydraulic tests, different thermo-hydro-mechanical and chemical processes occur at depth in the reservoir and could modify fluid pathways. In the vicinity of the re-injection well GPK3, a general cooling of the fractured rock mass associated with forced fluid flow provoking thermo-mechanical stresses is the dominant mechanism. Temperature reduction could also generate some chemical effects, inducing mineral dissolution or precipation, and thus strongly modifying the fluid pathway during circulation. Close to the production wells GPK2 and GPK4, pumping with submersible pumps could also induce some hydromechanical processes in the fractured rock mass. All these complex thermo-hydro-mechanical couplings will interact with the major fracture zone system and must be seriously investigated using modelling to estimate reservoir lifetime (temperature drawdown, microseismicity risk,

reservoir clogging). The fracture zone dataset studied in this paper could be used to model the thermo-hydraulic mechanical behavior of the deep geothermal granite reservoir subject to hydraulic or chemical stimulations and hydraulic circulations (Rachez and Gentier, 2008).

ACKNOWLEDGEMENTS

This work was performed as a contribution to the European Union's FP6 project 'Soultz EGS Pilot Plant' funded by ADEME (EGS3D projet), BMU, EC and EEIG 'Exploitation Minière de la Chaleur' and was supported by the Swiss State Secretariat for Education and Research under project number 03.04.60. EHDRA working group teams 6 and 7 are grateful for their contributions and the fruitful discussion.

REFERENCES

Baujard C. and Bruel D. (2005). Recent results on the impact of fluid density on the pressure distribution and stimulated area in the reservoir using a finite volume numerical code. Proceedings of the EHDRA scientific conference 14-18 March 2005, Soultz-sous-Forêts, France.

Baumgärtner J., Jung R., Gérard A., Baria R., Garnish J., (1996). The European HDR project at Soultz-sous-Forêts: stimulation of the second deep well and first circulation experiments. Twenty-first Workshop Geothermal Reservoir Engineering, Stanford University, Stanford, California, USA, 267-274.

Baumgärtner, J., Hettkamp T; Teza D., Baria R; and Michelet S. (2004). Building of a Hot Dry Rock scientific power plant at Soultz-sous-Forêts. Geothermal Resources Council Transactions, Vol. 28, 201-206.

Bruel, D., (2002). Impact of induced thermal stress during circulation tests in an engineered fractured geothermal reservoir. Oil & Gas Science and Technology, Revue IFP, 57, no. 5, 459-470.

Castera J., Dezayes Ch., Calcagno Ph., (2008). Large-scale 3D geological model around the Soultz site, Proceedings of the EHDRA scientific conference 24-25 September 2008, Soultz-sous-Forêts, France.

Cocherie A., Guerrot C., Fanning C.M., Genter A., (2004). Datation U-Pb des deux faciès du granite de Soultz (Fossé Rhénan, France). Comptes Rendus Geoscience, 336, 775-787.

Cuenot N., Charléty J., Dorbath L., Haessler H., (2006). Faulting mechanisms and stress regime at the European HDR site of Soultz-sous-Forêts, France, Geothermics, Vol. 35, No. 5-6, 561-575.

Dezayes Ch., Villemin Th., Genter A., Traineau H., Angelier J., (1995). Analysis of fractures in boreholes of the Hot Dry Rock project at Soultz-sous-Forêts (Rhine Graben, France). Scientific Drilling, vol. 5, 31-41.

Dezayes Ch., Villemin Th., Pêcher A., (2000). Microfracture pattern compared to core scale fractures in the borehole of Soultz-sous-Forêts granite, Rhine graben, France. Journal of Structural Geology, 22, 723-733.

Dezayes Ch., Genter A., Gentier S., (2004). Fracture network of the EGS Geothermal Reservoir at Soultz-sous-Forêts (Rhine Graben, France). Geothermal Resources Council Transactions, Palm Springs, California, USA, Vol. 28, 213-218.

Dezayes Ch., Valley B., Maqua E., Syren G., Genter A., (2005). Natural fracture system of the Soultz granite based on UBI data in the GPK3 and GPK4 wells. EHDRA Scientific Conference, Proceedings of the EHDRA scientific conference 17-18 March 2005, Soultz-sous-Forêts, France.

Dezayes Ch., Genter A., (2008). Large-scale fracture network based on Soultz borehole data. EHDRA Scientific Conference, Proceedings of the EHDRA scientific conference 24-25 September 2008, Soultz-sous-Forêts, France.

Dorbath L., Cuenot N., Genter A., Frogneux M., (2009). Seismic response of the fractured and faulted granite to massive water injection at 5 km depth at Soultz-sous-Forêts (France), Geophysical International Journal, doi: 10.1111/j.1365-246X.2009.04030.x

Evans K.F., (2000). The effect of the 1993 stimulations of well GPK1 at Soultz on the surrounding rock mass: evidence for the existence of a connected network of permeable fractures. World Geothermal Congress 2000, Kyushu - Tohoku, Japan.

Evans K.F., (2005). Permeability creation and damage due to massive fluid injections into granite at 3.5 km at Soultz: Part 2 - Critical stress and fracture strength, Journal of Geophysical Research, 110, B04204, 14 pp.

Evans K.F., Genter A., Sausse J., (2005). Permeability creation and damage due to massive fluid injections into granite at 3.5 km at Soultz: Part 1 - Borehole observations, Journal of Geophysical Research, 110, B04203, 19 pp.

Foehn J.P., (1985). Interprétation des campagnes sismiques 1981 et 1984, concession de Péchelbronn, permis de Haguenau. Total Exploration internal report, October 1985.

Genter A., (1989). Géothermie Roches Chaudes Sèches : le granite de Soultz-sous-Forêts (Bas Rhin, France). Fracturation naturelle, altérations hydrothermales et interaction eau - roche. PhD thesis, Université d'Orléans, France, 201 pp.

Genter A., Traineau H., Dezayes Ch., Elsass P., Ledésert B., Meunier A., Villemin Th., (1995). Fracture analysis and reservoir characterization of the granitic basement in the HDR Soultz project (France). Geothermal Science & Technology, vol. 4 (3), 189-214.

Genter A., Castaing C., Dezayes Ch., Tenzer H., Traineau H., Villemin Th., (1997). Comparative analysis of direct (core) and indirect (borehole imaging tools) collection of fracture data in the Hot Dry Rock Soultz reservoir (France), Journal of Geophysical Research, vol. 102, B7, 15419-15431.

Genter A., Castaing Ch., (1997). Effets d'échelle dans la fracturation des granites; Scale effects in the fracturing of granite. Comptes Rendus de l'Académie des Sciences, Serie II. Sciences de la Terre et des Planètes 325(6): 439-445.

Genter A., Homeier G., Chèvremont Ph., Tenzer H., (1999). Deepening of GPK-2 HDR borehole, 3880-5090 m (Soultz-sous-Forêts, France). Geological monitoring. Open file report BRGM/RR-40685-FR, 81 pp.

Genter A., Traineau H., Bourgine B., Ledésert B., Gentier S., (2000). Over 10 years of geological investigations within the European Soultz HDR project, France. Proceedings of the World Geothermal Congress 2000, Kyushu-Tohoku, Japan, May 28 - June 10, 2000, Full length paper on Cd-Rom, Editors E. Iglesias, D. Blackwell, T. Hunt, J. Lund, S. Tamanyu, 3707-3712.

Genter A., Cuenot N., Dezayes Ch., Sausse J., Valley B., Baumgartner J., Fritsch D., (2007). How a better characterization of a deep crystalline reservoir can contribute to improve EGS performance at Soultz, First European Geothermal Review, Geothermal Energy for Electric Power Production, October 29-31, 2007, Mainz, Rhineland Palatinate, Germany, Abstracts and Papers, 34-40.

Gérard A., Menjoz A., Schwoerer P., (1984), L'anomalie thermique de Soultz-sous-Forêts, Géothermie Actualités, n°3, 35-42.

Gérard A., Kappelmeyer O., (1987). The Soultz-sous-Forêts project: Proceedings of the first EEC/US workshop on geothermal Hot dry Rocks Technology, Geothermics, Special issue, 393-399.

Gérard A., Genter A., Kohl T., Lutz Ph., Rose P., Rummel F., (2006). The deep EGS (Enhanced Geothermal System) project at Soultz-sous-Forêts (Alsace, France). Geothermics, Vol. 35, No. 5-6, 473-483.

Herbrich B., (1988). Forage géothermiques de Soultz-sous-Forêts (GPK1). Rapport de fin de sondage. Rapport CFG n° 88 CFG 03, Janvier 1988.

Hooijkaas G.R., Genter A., Dezayes Ch., (2006). Deep-seated geology of the granite intrusions at the Soultz EGS site based on data from 5 km-deep boreholes, Geothermics, Vol. 35, No. 5-6, 484-506.

Illies H., (1972). The Rhine graben rift system - plate tectonic and transform faulting. Geophysical Survey, 1, 27-60.

Illies J.H., (1975). Recent and paleo-intraplate tectonics in stable Europe and the Rhinegraben rift system. Tectonophysics, 29, 251-264.

Jung R., Reich W., Engelking U., Hettkamp T., Weidler R., (1995). Hydraulic tests in1995 at the HDR Project, Soultz-sous-Forêts, France, Field Report, Bundesanstalt für Geowissenschaften und Rohstoffe (BGR), Hannover, Germany.

Klee G., Rummel F., (1993). Hydrofrac stress data for the European HDR research project test site Soultz-sous-Forêts. International Journal of Rock Mechanics and Mining Sciences & Geomechanics Abstracts 30(7): 973-976.

Kohl T. and Megel T. (2005). Numerical modelling of hydraulic stimulations at Soultz-sous-Forêts. Proceedings of the EHDRA scientific conference 17-18 March 2005, Soultz-sous-Forêts, France.

Le Carlier C., Royer J. J., Flores E. L. (1994). Convective heat transfer at Soultz-sous-Forêts geothermal site: implications for oil potential. *First Break*, **12**, 11, 553-560.

Ménillet F. et al. (1989). Carte géologique de Lembach à 1/50 000. Feuille n°168, Edition du BRGM.

Place J., Diraison M., Naville Ch., Geraud Y., Schaming M., Dezayes Ch., (2009). Decoupling of deformation in the Upper Rhine Graben sediments seen by seismic reflection and coupled analysis of diffraction on 3-component Vertical Seismic Profiling (Soultz-sous-Forêts area). *Geosciences*, accepted.

Rachez X., Gentier S., Blaisonneau A. (2006). Hydro-mechanical behaviour of GPK3 and GPK4 during the hydraulic stimulation tests – Influence of the stress field. Proceedings of the EHDRA scientific conference, Soultz-sous-Forêts, France.

Rachez X. and Gentier S. (2008). BRGM modeling activities performed at the Soultz EGS reservoir. Proceedings of the EHDRA scientific conference 24-25 September 2008, Soultz-sous-Forêts, France.

Renard Ph., Courrioux G., (1994). Three-dimensional geometric modelling of faulted domain: The Soultz horst example (Alsace, France). Computers & Geosciences, Vol. 20 (No. 9), 1379-1390.

Rotstein Y., Edel J. B., Gabriel G., Boulanger D., Schaming M., Munschy M., (2006). Insight into the structure of the Upper Rhine Graben and its basement from a new compilation of Bouguer Gravity, Tectonophysics, 425 (1-4), 55-70.

Sanjuan B., Rose P., Gérard A., Brach M., Braibant G., Foucher J.-C., Gauthier A., Touzelet S. (2005). Tracer testing using Naphthalene disulfonate componds during the stimulation operations carried out in the GPK2, GPK3 and GPK4 wells between 2003 and 2004 at Soultz-sous-Forêts (France). Proceedings of the EHDRA scientific conference 17-18 March 2005, Soultz-sous-Forêts, France.

Sanjuan B., Pinault J-L, Rose P., Gérard A., Brach M., Braibant G., Crouzet C., Foucher J-C, Gautier A., Touzelet S., (2006). Tracer testing of the geothermal heat exchanger at Soultz-sous-Forêts (France) between 2000 and 2005, Geothermics, Vol. 35, No. 5-6, 622-653.

Sausse J., Dezayes Ch., Dorbath L., Genter A., Place J., (2009). 3D fracture zone network at Soultz based on geological data, Image logs, microseismic events and VSP results, *Geosciences*, accepted.

Schill E. and Geiermann J. (2009). Identification of EGS resources in the Upper Rhine valley by magnetotellruic methods. *Geosciences*. Soumis

Stussi J.-M., Cheilletz J.M., Royer J.J., Chèvremont P., Féraud G., (2002). The hidden monzogranite of Soultz-sous-Forêts (Rhine Graben, France). Mineralogy, petrology and genesis, Géologie de la France, 1, 45-64.

Tenzer, H., Mastin, L. & Heinemann, B. (1991). Determination of planar discontinuities and borehole geometry in the crystalline rock of borehole GPK1 at Soultz-sous-Forêts. Geotherm. Sci. & Tech. 3(1-4), 31-67.

Valley B., (2007). The relation between natural fracturing and stress heterogeneities in deep-seated crystalline rocks at Soultz-sous-Forêts (France), PhD thesis, ETH-Zürich, Switzerland, http://e-collection.ethbib.ethz.ch/view/eth:30407, 260 pp.

Valley B., Dezayes Ch., Genter A., (2007). Multi-scale fracturing in the Soultz-sous-Forêts basement from borehole image analyses. Proceedings EHDRA Scientific Conference, 28 & 29 June 2007, Soultz-sous-Forêts, France, 14 pp.

Valley B., Evans K.F., (2007). Stress state at Soultz-sous-Forêts to 5 km depth from wellbore failure and hydraulic observations. Thirty-Second Workshop on Geothermal Reservoir Engineering Stanford University, Stanford, California, USA, January 28-30, 2008, SGP-TR-183, 329-338.

Villemin Th., Bergerat F., (1987). L'évolution structurale du fossé rhénan au cours du Cénozoïque : un bilan de la déformation et des effets thermiques de l'extension. Bull. Soc. Géol. France,, III, 2, 245-255

Villeneuve B., Weber R., (1991). Forages pour observations sismiques de Soultz-sous-Forêts. Rapport de fin de forages. BRGM-CCE.

Vuataz F.-D., Brach M., Criaud A., Fouillac Ch., (1990). Geochemical monitoring of drilling fluids: a powerful tool to forecast and detect formation waters. SPE, Formation Evaluation, June 1990, 177-184.

Ziegler P., (1992). European Cenozoic rift system. Tectonophysics, 2008, 91-111.